Tribology International 199 (2024) 110018

Contents lists available at ScienceDirect

Tribology International

journal homepage: www.elsevier.com/locate/triboint

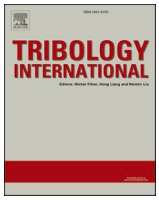

Correlating wear with the lubricant properties of heavy-duty diesel engine oils

Thomas Kirkby [a,*], Andrea Pacino [b], Joshua J. Smith [c], Mark Fowell [c], Jacqueline Berryman [c], Claes Frennfelt [d], Antonino La Rocca [b], Tom Reddyhoff [a,*]

[a] Tribology Group, Department of Mechanical Engineering, Imperial College London, London SW7 2AZ, UK
[b] Department of Mechanical Materials and Manufacturing Engineering, University of Nottingham, Nottingham NG7 2RD, UK
[c] Infineum UK Ltd, Milton Hill, Abingdon OX13 6BB, UK
[d] Volvo Group Trucks Technology, Göteborg, Sweden

ARTICLE INFO

Keywords:
Regression analysis
Soot
Wear
Detergent
ZDDP

ABSTRACT

Wear volumes were correlated with the lubricant properties of 11 used, heavy duty engine oil samples. The most important oil property in predicting wear volume is Total Acid Number, TAN. Here, the TAN value may be indicating ZDDP in its oxidised form and unable to participate in corrosive-abrasive wear. Low wear also correlates with mean soot particle size/circularity, which further suggests the abrasive aspect of this mechanism. Finally, low wear correlates with high calcium concentration in the fresh oil. This suggests a new wear reduction mechanism in which calcium from the detergent replenishes the iron within the ZDDP antiwear film.

1. Introduction

The importance of reducing polluting emissions has driven vehicle manufacturers to improve engine designs. Recent legislation means that emissions must be reduced [1], where one commonly used method is to optimise the combustion CO_2-NO_x trade-off. Reducing emissions is an especially important approach for heavy-duty vehicles as the energy limitations of current battery technologies mean that internal combustion engines will continue to be used for many years. However, this can lead to increased concentrations of soot in the oil – particularly with longer drain intervals - which in turn cause component durability problems due to high soot-mediated wear [2]. It is therefore important to understand, and thereby predict and reduce, the causes of wear in contacts lubricated by soot-containing oils. Many different soot-induced wear mechanisms have been suggested in the literature as summarised by Kirkby *et al.* [3]. These mechanisms can be categorised as being either physical, chemical or a combination of both.

Abrasive wear is a common physical mechanism associated with soot containing oils [2,4–12] whereby hard particles displace material from surfaces through erosion. However, the worn steel surfaces of components are often harder than the soot particles, which has led to the idea that it is the softer (and usually beneficial) zinc dialkyldithiophosphate (ZDDP) antiwear films that are abraded [13,14] (albeit supported mostly by studies testing carbon black rather than actual soot-containing oils – see combined mechanism discussed below). Lubricant starvation [6,7,15–18] is another commonly discussed mechanism for soot-containing oils, whereby particles accumulate at the contact inlet resulting in reduced fluid entrainment and increased metal-to-metal contact. This leads to other wear mechanisms such as: adhesive wear [11,14,17,19,20] where asperities touch and the resulting weld is sheared under a sliding motion, and fatigue wear [11,20–22] in which cracks form in the surface leading to material displacement. Soot particles may also be adsorbed on to the metal surface and prevent other antiwear additives from forming a protective film [17,23–25].

Chemical wear mechanisms associated with soot-containing oils can also occur, which include soot-additive interactions [8,26–30] and corrosive wear [2,20,31,32]. The latter usually involves the formation of weakly adhered oxides on the metal which can then be easily removed by rubbing. Soot particles can also function as nuclei for sulphuric acid to precipitate from the combustion process [33]. Exhaust gas recirculation (EGR) can increase the total acid number (TAN) by an increase of SO_x concentration [32]. Also, there may be high levels of surface disorder on soot particles due to unpaired electrons resulting in more chemical reactions and thus more wear [25]. Oil oxidises and degrades during its use in engines. Therefore, soot-accelerated oil degradation has been suggested and supported by studies in which engine oils were aged

* Corresponding authors.
E-mail addresses: t.kirkby20@imperial.ac.uk (T. Kirkby), t.reddyhoff@imperial.ac.uk (T. Reddyhoff).

https://doi.org/10.1016/j.triboint.2024.110018
Received 6 June 2024; Received in revised form 10 July 2024; Accepted 20 July 2024
Available online 22 July 2024

in the presence of carbon black [30].

The combined chemical-physical wear mechanism of corrosive-abrasion is also likely to occur [3,9,14,34–36]. This involves the formation of a ZDDP tribofilm, which is soft (compared to the metal substrate) and intermixed with the metal substrate, and its removal via by particle abrasion. This process happens continuously, with new ZDDP tribofilm being formed and subsequently abraded resulting in more and more wear. A recent study involving a single used, soot-containing, heavy-duty engine oil revealed the occurrence of this corrosive-abrasive wear mechanism [3]. However, a wider sample set must be used before concluding which mechanisms are most prevalent in practice, which is why this study correlates soot wear with the lubricant properties of multiple used, engine oils samples.

Despite progress in uncovering possible soot-induced wear mechanisms, it is still unclear which ones are most prevalent in real engines. Furthermore, most published research to date has studied carbon black-containing model lubricants rather than real, soot-containing engine oils. This raises the currently unanswered question of the suitability of carbon black as a soot surrogate. These shortcomings limit the design of lubricants that could reduce soot wear and are an obstacle to effective condition monitoring of oils since it is unknown which measurable lubricant properties best predict wear in practice.

In the context of internal combustion engines, soot specifically refers to carbonaceous particles that result from the incomplete combustion of fuel hydrocarbons [37]. Soot particulates are composed of nearly spherical small units known as "primary particles". These primary particles typically stick to one another forming branched aggregates. Most of the particulate matter leaves the cylinder with the exhaust gas, but a small proportion transfers into the engine oil via blow-by and thermophoretic mechanisms [38]. Transmission electron microscopy (TEM) is commonly used for soot characterisation [39–41]. Uy employed TEM to examine soot particulates from diesel and gasoline engines and found primary particles ranging from 8 to 43 nm in diameter [39]. Similarly, La Rocca *et al.* reported a mean diameter of 20 nm for particles extracted from diesel engine oil [40]. Slightly larger soot particulates in the range 30–100 nm were found by others [12,41]. Primary particles often collide to form soot aggregates with either branched or cluster-like morphology. These are typically between 50 and 500 nm depending on the formation conditions [41–43]. Due to the impact on oil performance and engine components, soot morphology is of interest in research [44–46]. For instance, aggregate area and particle size can significantly increase lubricant viscosity, resulting in oil control loss and pumpability concerns [44,45]. Similarly, larger wear volumes have been observed for larger primary particle sizes [46].

The situation is further complicated by the role of lubricant degradation in promoting wear, since this effect can be concurrent (and probably interconnected) with soot-induced wear. Therefore, being able to distinguish/disentangle oil degradation and soot effects would be beneficial in both increasing scientific understanding and enabling vehicle and lubricant manufacturers to target their research more effectively.

Engine dynamometer testing and field trials are costly and time consuming, therefore industries also use bench tests to rapidly assess the performance of oil formulations. One commonly used bench test is the high frequency reciprocating rig (HFRR) which simulates machine contacts that operate in the boundary regime. The harsh tribological conditions in this test generate an appreciable wear scar which can be analysed. The current study uses the HFRR to assess real engine oils with the aim of understanding the different mechanisms occurring and gain insights on how to test and develop better wear reducing lubricants. This is achieved by testing eleven used, soot-containing engine oil samples and then applying regression analysis to correlate the measured wear volumes with oil sample properties. Further surface analyses are then performed to test the hypotheses that arise from the regression findings.

2. Methods and materials

2.1. Obtaining regression data

2.1.1. Test lubricants

A set of 11 used oils: four from engine dynamometer testing and seven from field trial testing (labelled A to K), were selected covering a broad wear performance range. Three high frequency reciprocating rig test repeats were run for each oil. 55 different lubricant properties were measured, summarised in Table 1. This unprecedented amount of tribological and lubricant chemical data is given in the results section and appendices of this paper. As is expected with a large data set from real commercial samples, some data (13 % as shown in the Supplementary data) is unavailable as it was not measured during the industrial testing. Therefore, these oils were omitted from the regression analysis procedure when predicting functions that depended on missing variables and thus do not affect the resulting correlations. The full table of normalised values can be found in the Supplementary data.

2.1.2. Wear testing apparatus

The High Frequency Reciprocating Rig (HFRR; PCS Instruments Ltd.) was used to determine the coefficient of friction, boundary film coverage (measured via electrical contact resistance, ECR), and wear volume (Fig. 1). This rig is commonly used to screen lubricants as it rapidly and repeatably produces a rubbing contact operating in boundary lubrication simulating conditions found between engine components. A Mini-Traction Machine (MTM; PCS Instruments Ltd.) was also used to generate thicker tribofilms in a contact between a 19.05 mm diameter steel ball and 46 mm diameter steel disc which could be more easily analysed using scanning electron microscopy – energy dispersive x-ray (SEM-EDX). Standard HFRR and MTM specimens (properties shown in Table 2) were chosen in this study, since they are widely researched and produce well defined, repeatable wear scars that facilitated surface analyses. In practice, engine surfaces may have a greater roughness than

Table 1
Oil property standard test methods, where * indicates there was no standard method used, instead the machine is listed with a reference to the section detailing the procedure.

Property	Standard / Test Machine	Reference
HFRR wear volume (dependant variable)	HFRR*	Section 2.1.3
Coefficient of friction	HFRR*	Section 2.1.2
HFRR film coverage	HFRR*	Section 2.1.2
ICP elemental composition	ASTM D5185	[47]
Total acid number (TAN)	ASTM D664	[48]
Total base number (TBN)	ASTM D2896 and ASTM D4739	[49,50]
Soot Thermogravimetric analysis (TGA)	ASTM D5967	[51]
Soot Infrared (IR)	ASTM E2412	[52]
Oxidation	DIN51453 and ASTM E2412	[52,53]
Nitration	DIN51453 and ASTM E2412	[52,53]
KV40 and KV100	ASTM D445	[54]
Low temperature cranking viscosity (CCS)	ASTM D5293	[55]
High temperature high shear viscosity (HTHS)	ASTM D4683	[56]
Soot surface area	TEM*	Section 2.1.4
Soot circularity	TEM*	Section 2.1.4
Soot primary particle diameter	TEM*	Section 2.1.4
Soot tortuosity	TEM*	Section 2.1.4

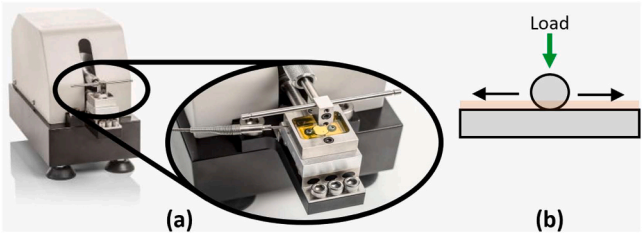

Fig. 1. (a) Picture of HFRR [58] and (b) schematic diagram of HFRR contact.

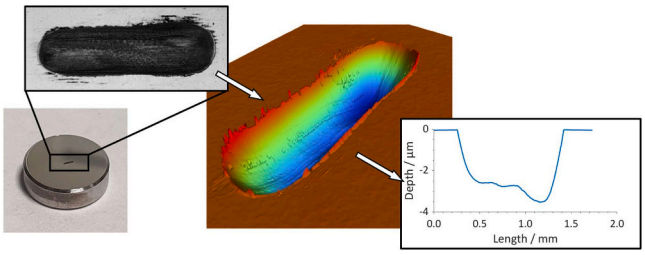

Fig. 2. HFRR wear scar volume determination from optical interferometry.

Table 2
HFRR and MTM test specimen properties.

	HFRR Ball	HFRR Disc	MTM Ball	MTM Disc
Material	AISI 52100 steel	AISI 52100 steel	AISI 52100 steel	AISI 52100 steel
Hardness / HV	690 – 890	190 – 210	800 – 920	720 – 780
Roughness,Ra / µm	< 0.05	< 0.02	< 0.05	< 0.02

this, which could affect both particle and ZDDP wear behaviour. It is also the case that 52100 steel of HFRR specimens differs from actual engine rocker-arm steel. However, an exploration of these roughness and metal composition effects is beyond the scope of this already large study and is subject of future research. It should also be noted that Pagkalis *et al.* [57] suggest that ZDDP antiwear film formation is not significantly influenced by steel composition or specimen surface roughness. The test specimen properties can be found in Table 2 and test conditions in Table 3.

The slide-roll ratio (SRR) is given by the equation:

$$SRR = \frac{2(u_b - u_d)}{(u_b + u_d)} \quad (1)$$

where u_b and u_d are the speeds of the ball and disc, respectively.

2.1.3. Wear measurement

After each wear test, oil present on the surface was removed by lightly rinsing with heptane. Then, wear scars were imaged and analysed using a Bruker Contour GT-K White Light Interferometer. Fig. 2 shows the method of wear scar volume determination; image → depth map → profile from which the wear scar volume is calculated.

2.1.4. Soot analysis

A solvent extraction procedure was used to separate soot from the engine oils. The dilution was conducted with an appropriate amount of heptane depending on the soot content in the sample. Small volumes of soot suspended in heptane were transferred onto carbon-coated transmission electron microscopy (TEM) grids. After deposition, the heptane evaporated, leaving soot aggregates and particles of various sizes. The grids were then cleaned with diethyl ether to remove any remaining oil contamination. The solvent was then vaporised by exposing the sample to near-vacuum conditions prior to the TEM session. Sonication and centrifugation steps were not used since they alter the size distribution of nanoparticles in the oil [40]. High-resolution images of soot on a copper mesh grid, composed of a holey amorphous carbon layer and a graphene oxide support film, were acquired using TEM. The imaging was conducted using a JEOL 2100 F TEM microscope equipped with a Gatan Orius CCD camera, located at the University of Nottingham's Nanoscale and Microscale Research Centre (nmRC). An incident electron beam voltage of 200 kV was used with various magnifications.

ImageJ software was used to study soot morphology. Multiple pictures for each sample were analysed to ensure a proper representation of the sample and to adjust for local variations. Samples were examined at various magnifications to investigate general soot morphology, aggregates, and primary particles. The evaluation of morphological data includes projected area, aggregate Feret diameter, primary particle size and tortuosity. Tortuosity is defined as the ratio of the length of the curve to the distance between its ends. A minimum of 100 primary particles per sample were collected and their diameters were assessed. Primary particle identification from TEM images was performed by a manual detection method. The morphological features of aggregates were assessed using a semi-automatic image processing approach developed in-house and coded in ImageJ. Before completing the binarization procedure, the aggregates were identified by manually selecting the soot particles and automatically adjusting the threshold.

Table 3
HFRR and MTM test conditions.

HFRR		MTM			
		Ball-on-disc rubbing step		Stribeck curve step	
Frequency / Hz	50	Slide roll ratio (SRR) / %	50	Slide roll ratio (SRR) / %	50
Ball load / N	3.92	Ball load / N	31	Ball load / N	31
Temperature / °C	100	Temperature / °C	100	Temperature / °C	100
Stroke length / mm	1	Entrainment speed / mm s^{-1}	50	Entrainment speeds / mm s^{-1}	3000 to 10
Test duration / h	1	Duration of step / min	15		

2.2. Regression method

Regression analysis is an applicable technique for finding correlations in experimental data between a single dependent and multiple possible independent variables. For instance, other studies have used regression analysis to compare between soot particle properties [59], however, these results have not then been compared to tribological results. Regression has also been used to correlate lubricant properties with engine efficiency [60–63] and engine parameters with soot emissions [64]. In the current study, how well the regression model fits the data suggests the significance of the property in predicting the wear scar volume. This is commonly referred to as the regression coefficient (R^2) ranging from 0 (no correlation between the properties) up to 1 (a perfect correlation). Multiple dependant variable regression analysis was also studied. This was done by identifying all the potential combinations and ranking the resultant correlations. An example equation, taken from [63], shows a two-variable regression:

$$ARKL\ EOTT = \quad 76.0 + (3110 \times MTM) + (0.0616 \times VI); \quad R^2 = 0.82 \quad (2)$$

where the dependant variable *ARKL EOTT* is the end-of-test temperature for the axial groove ball bearing tribometer test (achsialrillenkugellager, ARKL – known to predict gearbox efficiency in real vehicle engines), *MTM* is the friction measured using the Mini-Traction Machine, and *VI* is the viscosity index of the lubricant.

In this study, MATLAB was used to perform the regression analysis. Here, the oil properties were normalised between 0 and 1 using the min-

max normalisation equation:

$$x' = \frac{x - \min(x)}{\max(x) - \min(x)} \quad (3)$$

where x is the original value and x' is the normalised value. These normalised values were correlated with the normalised HFRR wear scar volume. Normalisation enables comparison between the magnitudes of the coefficients to suggest the relative contribution from each variable.

2.3. Surface characterisation methods

To probe the chemical composition of the wear scar surface, scanning electron microscopy – energy dispersive x-ray (SEM-EDX) data were recorded using a Zeiss SEM Auriga-45–24. High magnification SEM images of the surface were recorded using the secondary electron detector and elemental composition within the wear scar was recorded using the Oxford Instruments Z-Max 20 mm^2 EDX attachment at 5 keV.

A Helios 5 DualBeam FIB-SEM was used to prepare cross section samples of the wear scars for Scanning Transmission Electron Microscopy (STEM). The FIB-SEM deposits a platinum coating using a gallium ion source at 30 kV and 0.79 nA beam current, to a depth of 0.5 μm. Trenching (52 degrees) and undercutting (7 degrees) were performed using gallium ions at 30 keV and 21 nA current (Fig. 3b). Liftout performed using a Pt deposition and EasyLift micromanipulator (Fig. 3c). Deposition of lamella on TEM grid using Pt deposition (Fig. 3d). Thinning of TEM lamella by over-tilting (54 degrees) and under-tilting (50 degrees) and using a cleaning cross section to thin the lamella using 30 keV and decreasing current (2.5 nA, 0.79 nA, 0.43 nA, 0.23 nA) to a final thickness of 50–100 nm with polished sides (Fig. 3e).

The high resolution JEOL JEM 2100 F TEM was used to probe the structural characteristics of the film. The microscope was operated at 200 kV. Chemical characterisation was carried out using an EDS Oxford Instruments X-ray System INCA and spectra were collected between 0 and 10 kV.

3. Results

Wear scar volumes measured after the high frequency reciprocating rig (HFRR) testing of the eleven oils samples are presented in Fig. 4 (for each of the three repeat tests) and in Table 4 (averaged over the three repeats). Table 4 also presents four of the most influential oil properties, which have been selected due to their close correlations with wear scar volumes as reported below. A full set of these measured properties has been omitted from this results section for conciseness but can be found in the Supplementary data section.

3.1. Regression analysis

To check whether the "independent" variables were indeed independent of each other, correlations between all properties (not just with HFRR wear scar volume) were determined, (see results and discussion in the Supplementary data section). None of the correlations that arose in this general analysis were between variables that were highly correlated with wear scar volume. This suggests the relationships presented below can be taken at face value.

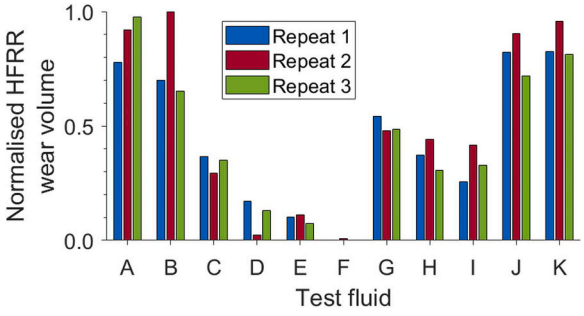

Fig. 4. HFRR wear scar volumes for all lubricants.

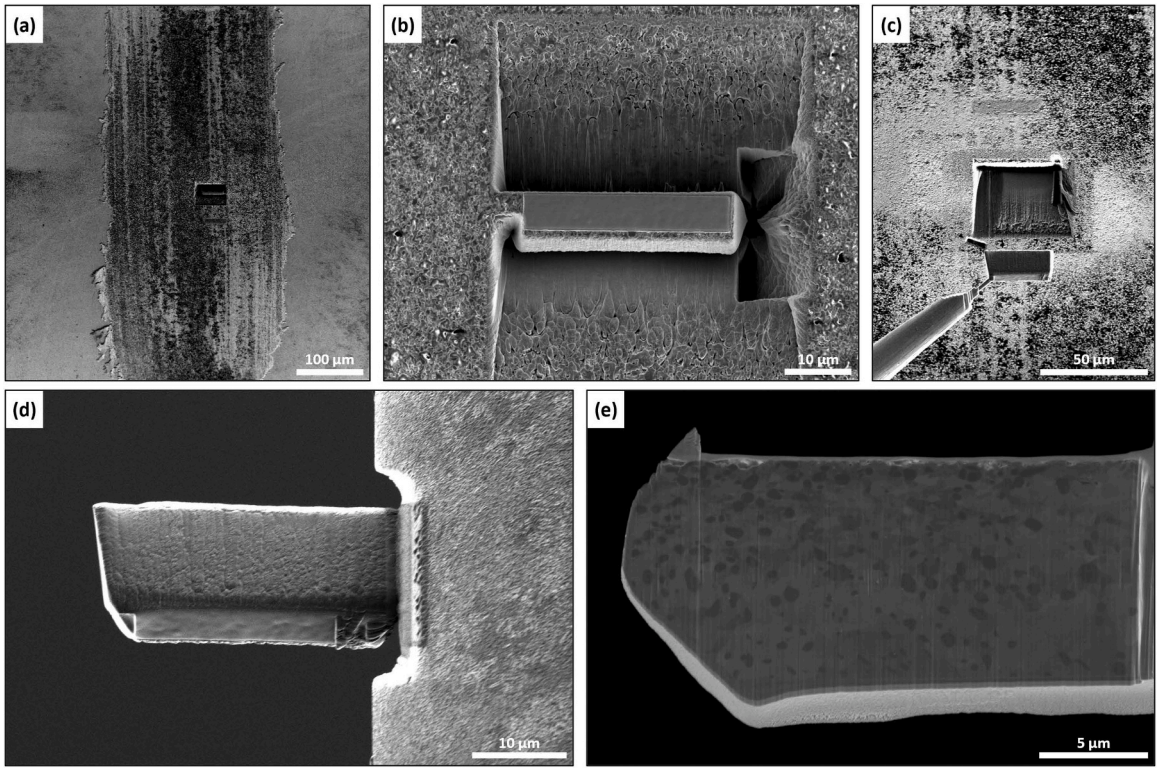

Fig. 3. STEM-EDX lamella preparation using the FIB-SEM where (a) is the full wear scar showing a small rectangle used for analysis, (b) trenching and undercutting, (c) liftout of the lamella, (d) deposition of the lamella on the TEM grid, and (e) thinning of the TEM lamella.

Table 4
Normalised average HFRR wear volumes and selected other lubricant property measurements, where SOT and EOT are the start- and end-of-test values, respectively (where the test referred to here is the engine or field test used to age the oil). All data is normalised between 0 and 1 within each property.

Test Fluid	Normalised average HFRR wear scar volume	Normalised total acid number (TAN) (EOT)	Normalised mean soot circularity	Normalised calcium concentration (SOT)	Normalised mean soot primary particle diameter
A	1.00	0.22	0.00	0.00	0.37
B	0.88	0.00	0.32	0.22	0.69
C	0.38	1.00	0.04	0.08	0.73
D	0.12	0.79	0.78	1.00	0.95
E	0.10	0.81	0.76	1.00	0.92
F	0.00	0.87	0.87	0.94	1.00
G	0.56	0.32	1.00	0.68	0.78
H	0.42	0.83	0.52	0.68	0.82
I	0.37	0.64	0.78	0.68	0.85
J	0.91	0.28	0.16	0.68	0.07
K	0.97	0.17	0.01	0.61	0.00

Regression analysis was then performed to determine the direct correlation between each single oil property and the normalised HFRR wear volume (*HFRR wear volume*′). This results in the equation in the form:

$$HFRR\ wear\ volume' = \quad a_0 + a_1 x_1' \tag{4}$$

where a_0 and a_1 are the fit coefficients and x_1' is the normalised independent variable. The top ten best single variable predictors are of wear scar volume are shown in Table 5, where total acid number (TAN) and soot properties are in first and second place respectively. A negative sign in the a_1 column denotes a negative correlation with wear (i.e., high TAN is associated with low wear), and vice versa.

Fig. 5a shows the normalised best correlated property, TAN, plotted against the normalised HFRR wear scar volume. The equation of the line is:

$$HFRR\ wear\ volume' = 0.9126 + (-0.8302 \times \mathrm{TAN(EOT)}') \tag{5}$$

where TAN(EOT)′ is the normalised end-of-test TAN measurement. Other key parameters in the wear mechanism related to soot appear repeatedly at the top of the correlation list. For instance, the soot primary particle size or circularity (as analysed by TEM) showed a negative correlation with wear scar volume, which were only marginally less statistically significant than that of total acid number (TAN). This implies that as soot particles increase in size and circularity, the wear volume decreases.

The ability to predict the wear scar volume *before* the oil is used in a vehicle would also be beneficial (especially for lubricant design). This can be assessed by finding the most influential property of fresh oil resulting from its formulation (rather than a used oil property which would be affected by the engine conditions that it is subjected to). Therefore, all the end-of-test (EOT) parameters were removed from the data set and the regression correlations were reranked. This shows that the concentration of magnesium and calcium together (which are grouped since these elements are both used in detergents) is the most influential property of fresh oil on wear scar volume (Fig. 5b). However, as expected, the R^2 value was much lower, 0.4327, compared to 0.7266 when the end-of-test parameters are included.

Table 5
Results from single-variable regression analysis correlation with HFRR wear volume, where SOT and EOT are the start- and end-of-test values, respectively (where the test referred to here is the engine or field test used to age the oil).

x_1'	a_0	a_1	p-value	R^2
Total acid number (TAN) (EOT)	0.9126	−0.8302	3.07×10^{-10}	0.7266
Mean soot primary particle diameter	0.9939	−0.8117	1.38×10^{-9}	0.6992
Sulphur (EOT)	0.0721	0.7828	1.56×10^{-6}	0.6573
Difference in Magnesium + Calcium (EOT-SOT)	0.0633	0.6922	3.24×10^{-6}	0.6341
Magnesium (EOT)	0.0140	0.7233	6.72×10^{-6}	0.6097
Boron (EOT)	−0.1244	0.7513	7.73×10^{-5}	0.5159
Mean soot circularity	0.7636	−0.6282	3.88×10^{-6}	0.5026
Average HFRR film coverage	0.7671	−0.5211	5.86×10^{-6}	0.4896
Magnesium + Calcium (SOT)	0.7846	−0.7251	3.19×10^{-5}	0.4327
Difference in total acid number (TAN) (EOT-SOT)	0.7672	−0.6236	2.97×10^{-4}	0.4136

To check the reliability of the above results, Table 5 also shows the p-values from the regression calculation. p-values (from Pearson's correlation) help to determine whether a relationship is observed in a larger population by testing a null hypothesis that the coefficient is equal to zero. Consequently, a smaller p-value is better as the null hypothesis can be rejected and the value is likely to be a meaningful addition to the model. All the best correlated properties have a p-value less than 0.05 and can be kept in the model. Furthermore, the values of the coefficient of determination (R^2) have been given to show how well each regression fits the experimental data. However, the data could still be nonlinear despite an acceptable R^2 [65]. Therefore, the residuals of the regression analysis were also studied and plotted against the fitted values, shown in Fig. 6. These residuals were calculated by subtracting each predicted value from each measured value and then plotted against the measured value. There is no correlation between the residuals which suggests linear regression is a suitable method of analysis for this data.

Regression analysis was then conducted using two independent variables. This enables an understanding of how multiple properties predict wear volume. The two variable correlations require combining independent variables to determine the HFRR wear volume, using the equation:

$$HFRR\ wear\ volume' = a_0 + a_1 x_1' + a_2 x_2' \tag{6}$$

where a_0, a_1 and a_2 are the fit coefficients and x_1' and x_2' are the normalised independent variables. The MATLAB code studied each of the 4032 possible combinations of independent variables and ranked them in terms according to the R^2 value. The ten best correlations are shown in Table 6.

The best correlation was again found to be the total acid number (TAN) in combination with the mean soot circularity, forming the equation:

$$HFRR\ wear\ volume' = 1.0123 + (-0.6636 \times \mathrm{TAN(EOT)}') + (-0.3985 \times SootCircularity') \tag{7}$$

where $TAN(EOT)'$ is the normalised end-of-test TAN measurement, and $SootCircularity'$ is the normalised mean soot circularity. To visualise this correlation, the combined independent variables are plotted against normalised HFRR wear scar volume using Eq. 7 (Fig. 7a). There is an increase in the R^2 value to 0.8996 compared with the best single variable equation (R^2 = 0.7266) and no correlation is seen in the residuals (Fig. 7b).

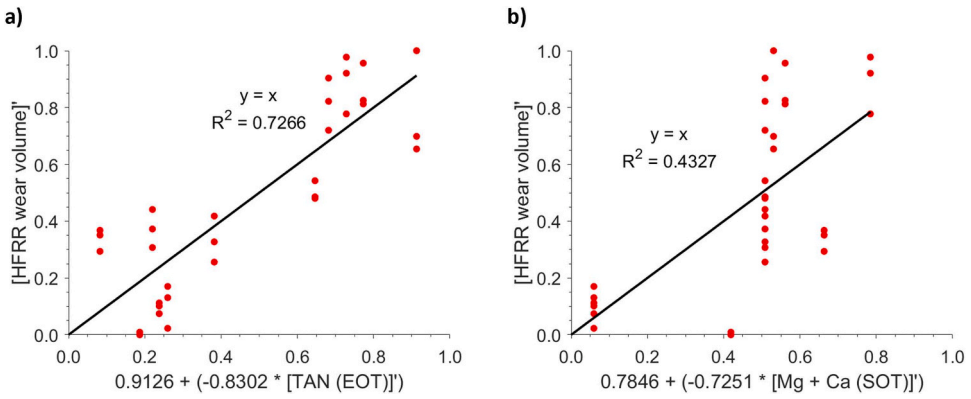

Fig. 5. (a) Wear scar volume vs. the best correlating variable, end-of-test total acid number (TAN (EOT)) (including the end-of-test values) and (b) with the combination of the magnesium and calcium start-of-test concentrations (Mg + Ca (SOT)) (excluding the end-of-test values).

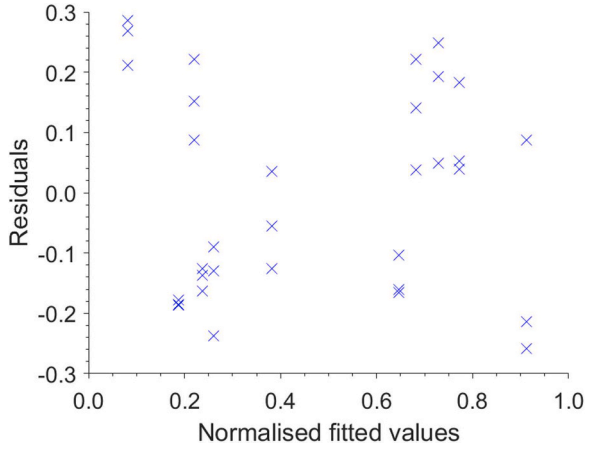

Fig. 6. Residuals from one variable regression analysis correlating normalised HFRR wear volume and TAN (EOT).

Three variable regression analysis was also conducted with the normalised HFRR wear volume forming the equation:

$$HFRR\ wear\ volume' = a_0 + a_1 x_1' + a_2 x_2' + a_3 x_3' \quad (8)$$

where a_0, a_1, a_2 and a_3 are the fit coefficients and x_1', x_2' and x_3' are the normalised independent variables. Table 7 shows the top ten highest correlating results from this analysis.

The best correlation with normalised HFRR wear volume again involves TAN in addition to the mean soot primary particle diameter and the calcium start-of-test concentration. This is represented by the equation:

$$HFRR\ wear\ volume' = 1.1424 + (-0.4461 \times \mathrm{TAN(EOT)}') + (-0.4120 \times SootPP') + (-0.2825 \times Calcium(\mathrm{SOT})') \quad (9)$$

where $TAN(EOT)'$ is the normalised end-of-test TAN measurement, $SootPP'$ is the normalised mean soot primary particle diameter, and $Calcium(SOT)'$ is the normalised calcium concentration measured at the start of the test. This resulted in an R^2 of 0.9291 which is a further improvement from the two-variable analysis ($R^2 = 0.8996$). Fig. 8 plots the combined independent variables against the normalised HFRR wear scar volume (Eq. 9), with no correlation of residuals.

3.2. Surface analysis

To study the unexpected prominence of calcium in the regression analysis results, ball-on-disc MTM wear tests were conducted on a fresh unused oil and an oil which had been aged in an engine test. The wear test conducted on a fresh unused oil resulted in an antiwear film (Fig. 9a) which contained calcium from the detergent (as detected by SEM-EDX in Fig. 9c) (as well as zinc which is expected from the ZDDP). However, the wear test on the same oil formulation after it has been aged in an engine, resulted in no antiwear film (see SEM image in Fig. 9b) and no calcium was present on the surface (as shown by EDX in Fig. 9d), despite the presence of calcium in the bulk of the oil (as confirmed by ICP data). Similarly, magnesium (an alternative to calcium in detergents, which showed up in the two and three variable models), is present in the fresh antiwear film (Fig. 9c), but not on the used worn surface (Fig. 9d).

Additional HFRR wear tests were conducted on a fresh fully formulated oil (FF) and a fresh fully formulated oil without detergent (FF without detergent) to remove any calcium or magnesium from the

Table 6
Results from two-variable regression analysis correlation with HFRR wear volume, where SOT and EOT are the start- and end-of-test values, respectively, PP is primary particle, HTHS is the high temperature high shear viscosity, and CCS is the low temperature cranking viscosity.

x_1'	x_2'	a_0	a_1	a_2	R^2
Total acid number (TAN) (EOT)	Mean soot circularity	1.0123	−0.6636	−0.3985	0.8996
Total acid number (TAN) (EOT)	Mean soot PP diameter	1.0502	−0.5180	−0.4694	0.8577
Total acid number (TAN) (EOT)	Magnesium + Calcium (SOT)	1.0153	−0.6828	−0.4128	0.8439
Total acid number (TAN) (EOT)	Calcium (SOT)	1.0425	−0.6991	−0.3366	0.8308
Total acid number (TAN) (EOT)	Average HFRR film coverage	0.9710	−0.6523	−0.2659	0.8207
Mean soot PP diameter	Calcium (SOT)	1.1193	−0.6802	−0.3543	0.8163
Total acid number (TAN) (EOT)	Iron (EOT)	0.8055	−0.8273	0.3106	0.8153
Total acid number (TAN) (EOT)	HTHS (SOT)	0.9250	−0.7499	−0.3040	0.7834
Total acid number (TAN) (EOT)	Copper (EOT)	0.9782	−0.8212	−0.2660	0.7803
Total acid number (TAN) (EOT)	CCS (SOT)	0.9949	−0.8128	−0.3158	0.7803

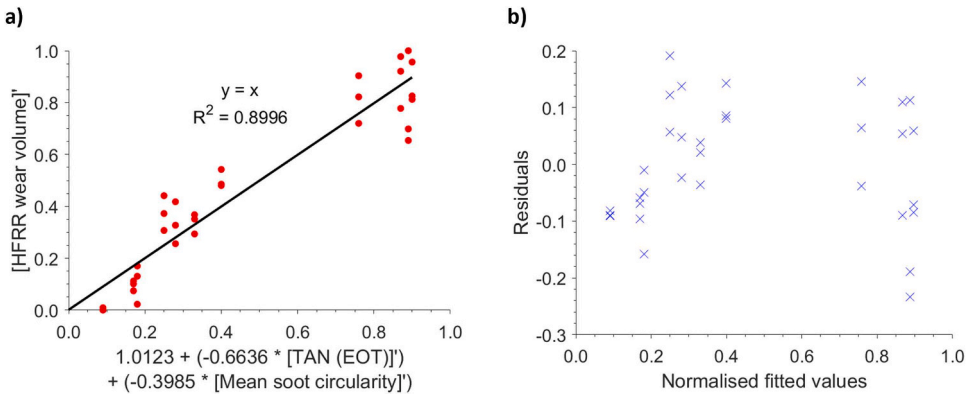

Fig. 7. **(a)** Wear scar volume vs. the two best correlating variables of total acid number (TAN) and mean soot circularity and **(b)** Residuals from regression analysis vs. the fitted values.

Table 7
Results from three-variable regression analysis correlation with HFRR wear volume, where SOT and EOT are start- and end-of-test values, respectively, TAN is the total acid number, TBN is the total base number, PP is primary particle, and CCS is the low temperature cranking viscosity.

x_1'	x_2'	x_3'	a_0	a_1	a_2	a_3	R^2
TAN (EOT)	Mean soot PP diameter	Calcium (SOT)	1.1424	−0.4461	−0.4120	−0.2825	0.9291
TAN (EOT)	Mean soot circularity	Copper (EOT)	0.9876	−0.5892	−0.6010	0.3056	0.9258
TAN (EOT)	Mean soot circularity	Magnesium + Calcium (SOT)	1.0394	−0.6297	−0.3126	−0.1953	0.9178
TAN (EOT)	Mean soot circularity	Magnesium (SOT)	1.0573	−0.6433	−0.4089	−0.1166	0.9169
TAN (EOT)	Mean soot circularity	Soot TGA	1.1231	−0.6752	−0.5072	−0.1463	0.9131
TAN (EOT)	Mean soot PP diameter	Magnesium + Calcium (SOT)	1.0930	−0.4830	−0.3609	−0.3000	0.9126
TAN (EOT)	Mean soot circularity	TBN (SOT)	0.9829	−0.6645	−0.4484	0.0958	0.9094
TAN (EOT)	Mean soot circularity	Sulphur (SOT)	1.0954	−0.7010	−0.4412	−0.1335	0.9093
TAN (EOT)	Mean soot circularity	CCS (SOT)	1.0379	−0.6700	−0.3660	−0.1291	0.9074
TAN (EOT)	Mean soot circularity	Mean soot PP diameter	1.0362	−0.5969	−0.3144	−0.1532	0.9058

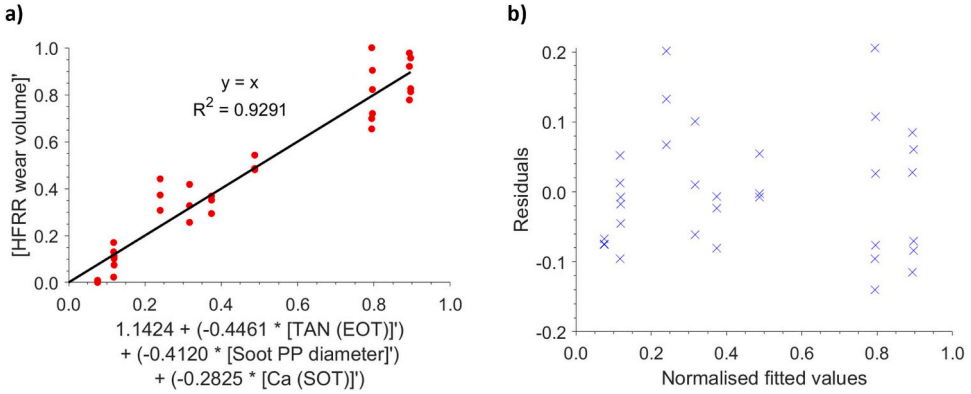

Fig. 8. (a) Wear scar volume vs. the three best correlating variables of the TAN end-of-test value, mean soot primary particle (PP) diameter and the calcium (Ca) start-of-test concentration and (b) plot of the residuals from the regression analysis.

system. Then, STEM-EDX was used to determine the elemental concentration on the surface. As shown in Fig. 10, there is a difference between the two films. The specimen surface from the fresh, fully formulated oil test has, as expected, more calcium and magnesium present than that from the oil without detergent. The film contains complementary locations of calcium, magnesium, phosphorus, and oxygen with the inverse locations of zinc and sulphur in the film. These film containing elements are all directly inverse to the iron, chromium, and manganese maps for both samples.

The iron and calcium concentrations were studied further to understand the influence of calcium in the film. To enable a good comparison between the tests, the STEM-EDX data was divided by the total number of counts and then normalised between 0 and 1. The area was calculated under the calcium Kα peak (around 3.69 keV) and iron Kα peak (around 6.40 keV). Fig. 11 shows these normalised elemental concentration changes across the depth of the film and the metal. The fresh oil without detergent showed an approximately constant iron intensity between the specimen surface and the film, while the fully formulated (FF) oil showed a large immediate decrease in iron intensity and an increase in calcium intensity moving from the specimen into the film.

4. Discussion

The most prominent property in the regression analysis correlations is the total acid number (TAN) at the end of the test is, followed by the soot properties, as summarised in Table 8. As all the regression coefficients have been normalised, their magnitude and sign can be

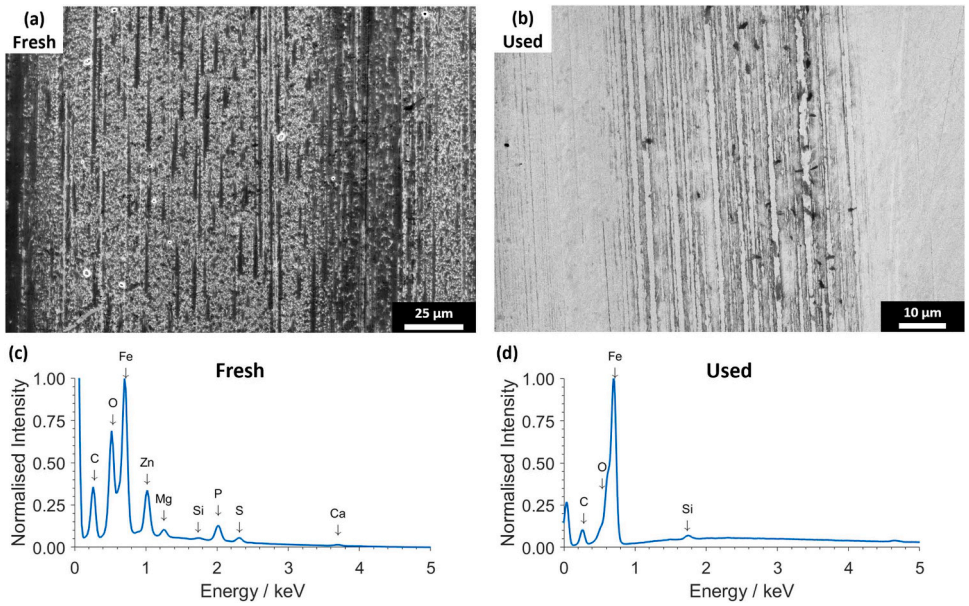

Fig. 9. SEM images of the MTM wear scar of (a) the fresh, unused, fully formulated oil and (b) the used soot-containing oil, and normalised SEM-EDX spectra of the MTM wear scars of (c) the fresh, unused, fully formulated oil and (d) the used soot-containing oil.

compared with each other to determine the proportion of their contribution. For the two-variable analysis, there is a larger contribution from the total acid number (TAN) than the soot circularity. For the three-variable analysis involving the total acid number (TAN) and the soot primary particle diameter, there is an almost even contribution, while there is less of a contribution from calcium.

A negative correlation is observed between the total acid number (TAN) and the HFRR wear scar volume which suggests that a decrease in TAN results in an increase in the wear volume. Aldajah *et al.* observed the same trend when looking at the wear from engine test samples [2]. When either the soot circularity or the soot primary particle diameter decreases, the wear volume increases. This suggests that the smaller, or flatter particles are more capable of wearing down the surfaces, which is likely due to the increased abrasive ability of smaller soot particles to wear the surfaces. Alternatively, larger, or more circular particles may indicate the beneficial presence of dispersant around the soot. Soot TGA concentration only appears once in the correlations which suggests that the soot concentration may not be directly related to the wear volume. Previous authors have stated that total acid number and soot particles may be closely related to each other as Kagaya suggested that the removal of soot resulted in a decrease in TAN [66]. Also, Sato *et al.* concluded that TAN increased due to carbon black absorbing acidic products but correlated TAN with wear volume [67]. However, TAN did not correlate with soot concentration (seen in the general correlations in the Supplementary data). Instead, TAN is more closely related to ZDDP film formation as discussed below.

In high TAN environments, ZDDP may be performing more of an antioxidant role rather than antiwear role [68,69]. ZDDP can prevent the oil from oxidising through its ability to inhibit peroxides and scavenge radicals and, in doing so, degrades into dithiophosphate, mono- and di-sulphides, and $ZnSO_4$ or ZnO [68]. Interestingly, in these degraded forms, ZDDP is less able to form an antiwear film [68,70]. These two previous findings are relevant since the corrosive-abrasive wear mechanism, suggested previously [3] for soot-containing oils, involves the formation of a relatively soft ZDDP tribofilm which is then abraded away by soot particles, thus removing the intermixed iron surface. Therefore, in our study, high TAN may be indicating that ZDDP has performed more of an antioxidant role which depletes its effectiveness as an antiwear additive and so it forms surface films less rapidly. This instance of high TAN being associated with low wear may be counterintuitive considering its usual association with high levels of base oil oxidation and likely degradation of other oil components. There are several possible reasons for this apparent discrepancy. For instance, the corrosive-abrasive wear mechanism favoured by the soot-containing oils obtained under the test conditions used in this study may be exacerbated by higher antiwear ZDDP concentration (i.e., low TAN). However, other oils that are heavily oxidised without high concentrations of soot may favour other mechanisms such as pure abrasive wear that are likely to be associated with low antiwear additive concentration (i.e., high TAN).

The test lubricants were harvested at a single point within each engine's operation. However, clearly the engine oil properties, and hence wear performance, evolve between drain intervals depending on the instantaneous time history of the oil. At the start, the fresh oil will have zero soot and virtually zero TAN. As the oil ages, soot will accumulate, and the TAN will increase. Then, at the end of the oil drain interval, highest levels of soot content may be expected along with highest TAN values. Together this suggests that the highest wear will likely occur somewhere in the first half of the oil drain interval when moderate levels of both soot and ZDDP are present (the latter indicated by high TAN).

Calcium was the most important variable after TAN and soot properties, correlating highly in the three-variable regression (Table 8 and Fig. 8a) and the single start-of-test regression (in combination with magnesium, Table 8 and Fig. 5b). In each case, there is a negative correlation which suggests that an increase in calcium results in a decrease in the wear volume. This is likely due to the detergent cations from the engine oil (there are no other sources of calcium in the oils tested) which are known to become integrated into any ZDDP antiwear tribofilm that is formed [71,72]. This was shown in Fig. 9 where calcium was found in the film formed from a fresh unused oil, but not in the film of a used oil. Furthermore, the STEM-EDX measurements (Fig. 11) after rubbing in fresh, fully formulated oil (FF) showed a large immediate decrease in iron intensity and an increase in calcium intensity in the direction from the disc metal into the film. In contrast, the fresh fully formulated oil without detergent showed only a very small decrease in iron intensity between the metal and the film probably due to the formation of iron sulphide retaining iron in the film [35]. This shows that there is more calcium and less iron in the film from the fully formulated oil. This all supports the theory that the detergent is required for enhanced wear protection. There are two possible mechanisms for this:

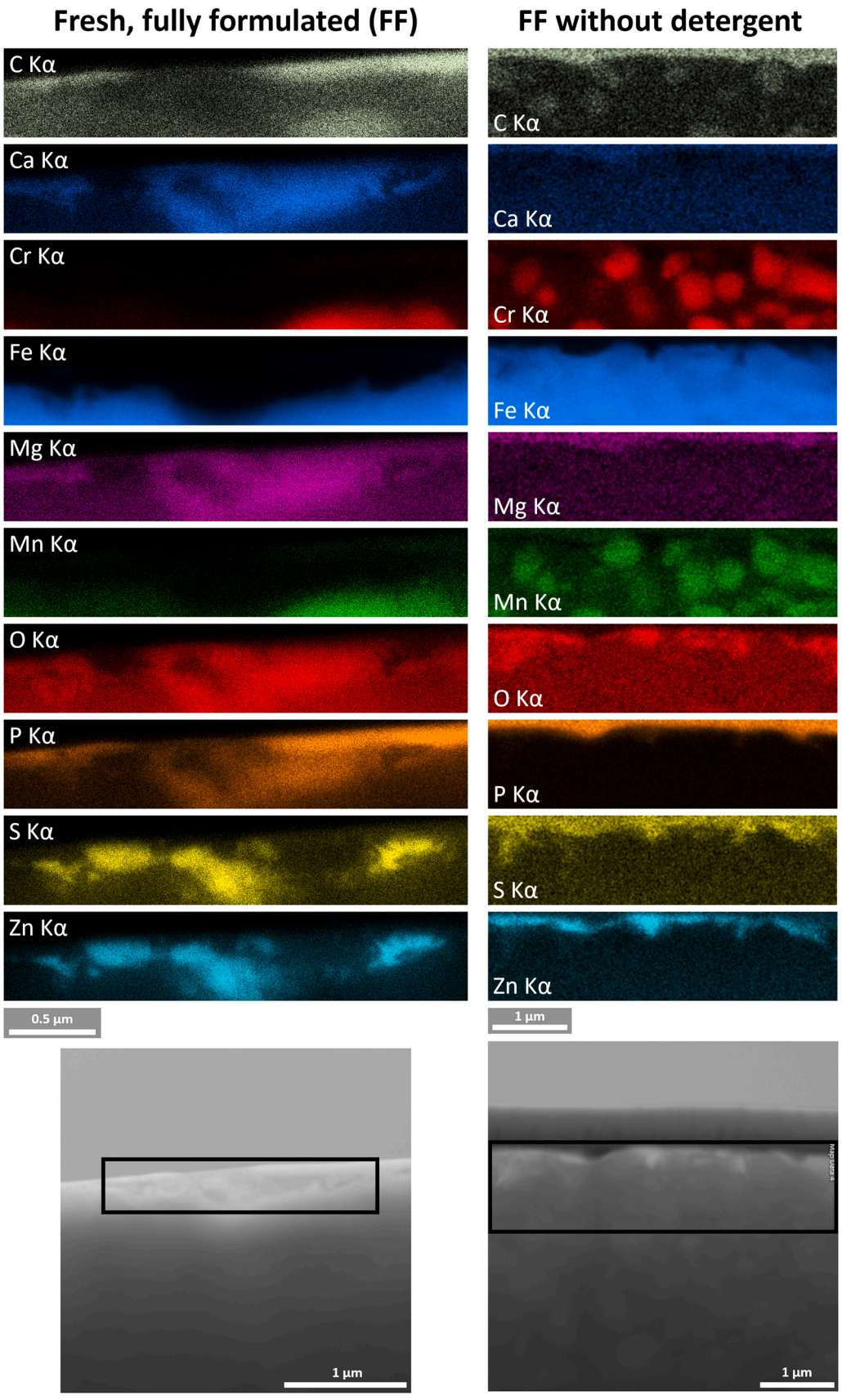

Fig. 10. STEM-EDX maps of the surface of the HFRR wear scar after testing (EDX elemental maps shown above, TEM image of location shown below) using a fresh fully formulated oil (FF, left) and a fresh fully formulated oil without detergent (FF without detergent, right).

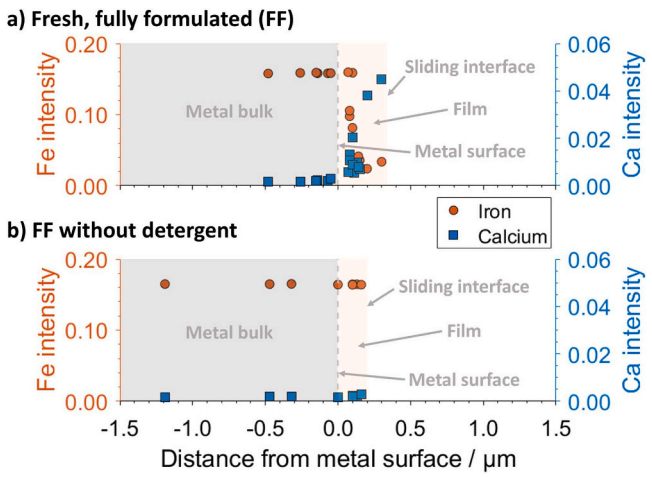

Fig. 11. Normalised iron and calcium concentrations across the depth of the HFRR wear scar for **(a)** the fresh, fully formulated oil (FF) and **(b)** the fresh, fully formulated oil without detergent.

i) Calcium may be hardening the tribofilm making it more difficult to be abraded, resulting in less wear. However, this theory is challenged by the observation that rubbing tests in used oil produced surfaces without any tribofilm elements on them so there is no anti-wear film for the calcium to harden (Fig. 8). As tribofilm elements are present in the oil, a film should form. This theory suggests that as calcium hardens this film to prevent wear, the film should be visible at the end of the test as it is not worn away. This is not observed; hence another theory is required, as discussed below.

ii) Calcium ions (from the detergent) compete with the iron ions (from the steel specimen) to balance the negatively charged species during antiwear film formation [73,74] (illustrated in Fig. 12). Therefore, subsequent abrasion of the film carries away less iron from the steel component surface (and more calcium originating from within the oil). This is beneficial since the resulting depletion of calcium is less problematic and more cheaply/easily remediable (e.g., by increasing detergent concentration) compared costly component wear. This newly proposed mechanism is supported by observations that: (a) when components are rubbed together in fresh, soot-free oil, calcium is incorporated into the antifilm at the expense of iron from the surface (Fig. 10, and [71,72]), and (b) when components are rubbed together in used soot-containing oil, wear decreases with increasing calcium despite no calcium being detected on the worn surface (Fig. 9).

5. Conclusion

Soot-mediated wear in heavy-duty diesel engines cause component durability problems, which can be mitigated by reducing soot concentrations in oil. However, this places limits on combustion parameters which could otherwise be optimised to reduce CO_2 emission from vehicles that are too large to be powered by current battery technology. Other solutions may be implemented if the underlying soot wear mechanisms (of which many have been proposed but from studies of model oils containing artificial soot) are better understood.

The results of this study, which correlated lubricant properties with wear volume from a sliding contacts lubricated by real soot-containing heavy-duty engine oils, are all congruent with the hypothesis that a corrosive-abrasive wear mechanism is occurring under our test conditions. Whereby the antiwear additive ZDDP forms a surface film, which incorporates iron from the metal below, and is repeatedly worn away by the abrasive action of soot [3].

The single most important oil property in predicting HFRR wear volume is the Total Acid Number, TAN (i.e., the amount of base needed to neutralise a quantity of sample). Specifically, a decrease in TAN results in an increase in wear volume, with an $R^2 = 0.7266$. Here, high TAN may be indicating that ZDDP has performed more of an antioxidant role [68,69] which depletes its effectiveness as an antiwear additive and so its relatively soft, abradable tribofilm forms less rapidly and thus slows the prevailing corrosive-abrasive mechanism. Also, when either the soot circularity or the soot primary particle diameter decreases, the

Table 8
Summary of the best correlated regression results, where TAN is the total acid number and PP is primary particle.

x_1'	x_2'	x_3'	a_0	a_1	a_2	a_3	R^2
TAN (EOT)			0.9126	−0.8302			0.7266
TAN (EOT)	Mean soot circularity		1.0123	−0.6636	−0.3985		0.8996
TAN (EOT)	Mean soot PP diameter	Calcium (SOT)	1.1424	−0.4461	−0.4120	−0.2825	0.9291

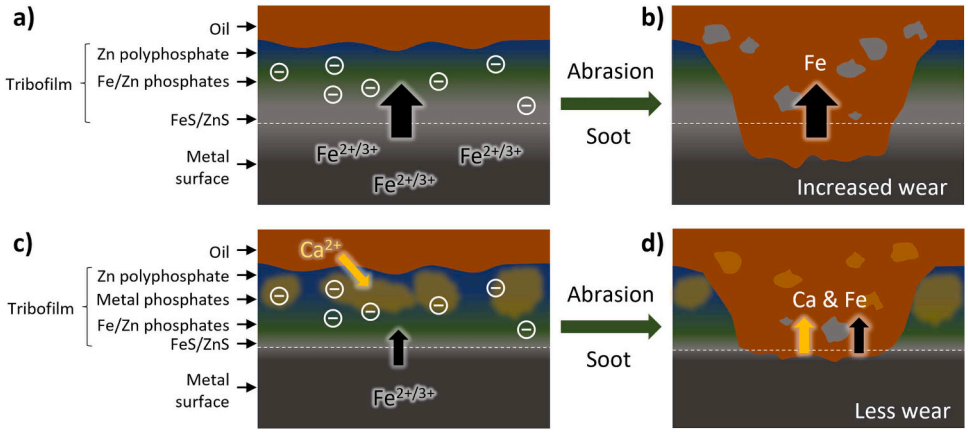

Fig. 12. Cartoon adapted from [68] to show role of calcium in mitigating corrosive-abrasive wear: (a) no calcium is present in the oil so that only iron is intermixed into the tribofilm, (b) subsequent soot abrasion of the film carries away metal from the steel component, (c) calcium from the detergent is present in the oil and becomes integrated into the tribofilm at the expense of iron from the steel surface, (d) subsequent soot abrasion of the film carries away less metal from the steel component.

wear volume increases. This may be due to the increased abrasive ability of smaller soot particles to wear the surfaces.

Calcium concentration is the start-of-test variable (i.e., one that can be measured before use) which most influences wear volume. There is a negative correlation suggesting that an increase in calcium results in a decrease in wear. This suggests a new wear reduction mechanism in which calcium within the lubricant replenishes the iron within the ZDDP antiwear film and thus reduces the amount of metal removed from the component's surface. This is supported by the following observations: (i) detergent cations from the engine oil are known to become integrated into any ZDDP antiwear tribofilm that is formed [71,72], since calcium ions compete with the iron ions during tribofilm formation to balance the negatively charged species [73,74], (ii) surface analysis EDX measurements showed that there was no tribofilm present. This suggests that increasing calcium concentration may be an effective way to reduce corrosive-abrasive wear and help ZDDP function more effectively. This important since ZDDP is a vital additive in any engine oil formulation without which seizure would rapidly occur.

These findings aid the design of lubricants (by showing what additives best limit wear) and the development of condition monitoring systems (by highlighting which oil properties are predict high wear).

Statement of originality

The research work described in this paper is, to the best of our knowledge and belief, original, except as referenced and acknowledged in the text. The work has not been submitted elsewhere, either in whole or in part, for publication.

CRediT authorship contribution statement

Mark Fowell: Writing – review & editing, Supervision. **Joshua J Smith:** Writing – review & editing, Supervision. **Jacqueline Berryman:** Writing – review & editing, Supervision. **Andrea Pacino:** Writing – review & editing, Data curation. **Thomas Kirkby:** Writing – review & editing, Writing – original draft, Methodology, Investigation, Formal analysis, Data curation. **Antonino La Rocca:** Writing – review & editing, Supervision. **Claes Frennfelt:** Writing – review & editing, Supervision, Funding acquisition. **Tom Reddyhoff:** Writing – review & editing, Visualization, Validation, Supervision, Project administration, Funding acquisition, Conceptualization.

Declaration of Competing Interest

The authors have no interests relating to this paper to declare.

Data availability

Data will be made available on request.

Acknowledgements

This work was funded by Volvo Group Trucks Technology. The help and assistance of Miss Jessica Tjandra on the TEM lamella sample preparation using the focused ion beam SEM (FIB-SEM) and of Mr Di Wang on the TEM are both greatly appreciated. Insightful discussions with Prof Hugh Spikes were also beneficial.

Appendix A. Supporting information

Supplementary data associated with this article can be found in the online version at doi:10.1016/j.triboint.2024.110018.

References

[1] The European Parliament, PE-CONS 109/23 Regulation (EU)2024 of the European Parliament and of the Council on type-approval of motor vehicles and engines and of systems, components and separate technical units intended for such vehicles, with respect to their emissions and battery durability (Euro 7), 2024.
[2] Aldajah S, Ajayi OO, Fenske GR, Goldblatt IL. Effect of exhaust gas recirculation (EGR) contamination of diesel engine oil on wear. Wear 2007;263:93–8. https://doi.org/10.1016/j.wear.2006.12.055.
[3] Kirkby T, Smith JJ, Berryman J, Fowell M, Reddyhoff T. Soot wear mechanisms in heavy-duty diesel engine contacts. Wear 2023:204733. https://doi.org/10.1016/j.wear.2023.204733.
[4] I. Nagai, H. Endo, H. Nakamura, H. Yano, Soot and Valve Train Wear in Passenger Car Diesel Engines, SAE Technical Papers (1983). https://doi.org/10.4271/831757.
[5] Ryason PR, Chan IY, Gilmore JT. Polishing wear by soot. Wear 1990;137:15–24. https://doi.org/10.1016/0043-1648(90)90014-2.
[6] Green DA, Lewis R, Dwyer-Joyce RS. Wear effects and mechanisms of soot-contaminated automotive lubricants. Proc Inst Mech Eng, Part J: J Eng Tribology 2006;220:159–69. https://doi.org/10.1243/13506501JET140.
[7] Penchaliah R, Harvey TJ, Wood RJK, Nelson K, Powrie HEG. The effects of diesel contaminants on tribological performance on sliding steel on steel contacts. Proc Inst Mech Eng, Part J: J Eng Tribology 2011;225:779–97. https://doi.org/10.1177/1350650111409825.
[8] Schilowitz AM, Konicek AR. Role of zinc dialkyl dithiophosphate in carbon black induced abrasive wear. Wear 376–377 2017:771–6. https://doi.org/10.1016/j.wear.2017.01.054.
[9] Kontou A, Southby M, Spikes HA. Effect of steel hardness on soot wear. Wear 390–391 2017:236–45. https://doi.org/10.1016/j.wear.2017.07.020.
[10] Patel M, Aswath PB. Role of thermal, mechanical and oxidising treatment on structure and chemistry of carbon black and its impact on wear and friction: part 2 – boundary lubrication condition. Tribology - Mater, Surf Interfaces 2015;9:19–32. https://doi.org/10.1179/1751584×14Y.0000000087.
[11] P. Rungsritanapaisan, P. Karin, W. Amornprapa, D. Tanprayoon, R. Tongsri, K. Hanamura, Impact of Soot and Engine Oil Additive Characteristics on Metallic Wear using Electron Microscopy and Confocal Microscopy, SAE Technical Papers 2019–32-0601 (2020).
[12] R. Mainwaring, Soot and Wear in Heavy Duty Diesel Engines, in: SAE Technical Papers, 1997. https://doi.org/10.4271/971631.
[13] Ratoi M, Castle RC, Bovington CH, Spikes HA. The influence of soot and dispersant on ZDDP film thickness and friction. Lubr Sci 2004;17:25–43. https://doi.org/10.1002/ls.3010170103.
[14] Olomolehin Y, Kapadia R, Spikes H. Antagonistic interaction of antiwear additives and carbon black. Tribol Lett 2010;37:49–58. https://doi.org/10.1007/s11249-009-9489-4.
[15] Yoshida K. Effects of sliding speed and temperature on tribological behavior with oils containing a polymer additive or soot. Tribology Trans 1990;33:221–8. https://doi.org/10.1080/10402009008981950.
[16] Colacicco P, Mazuyer D. The role of soot aggregation on the lubrication of diesel engines. Tribology Trans 1995;38:959–65. https://doi.org/10.1080/10402009508983493.
[17] Hu E, Hu X, Liu T, Fang L, Dearn KD, Xu H. The role of soot particles in the tribological behavior of engine lubricating oils. Wear 2013;304:152–61. https://doi.org/10.1016/j.wear.2013.05.002.
[18] H. Sato, N. Tokuoka, H. Yamamoto, M. Sasaki, Study on Wear Mechanism by Soot Contaminated in Engine Oil (First Report: Relation Between Characteristics of Used Oil and Wear), in: S.A.E. Technical Papers, 1999. https://doi.org/10.4271/1999–01-3573.
[19] Vyavhare K, Bagi S, Patel M, Aswath PB. Impact of diesel engine oil additives–soot interactions on physiochemical, oxidation, and wear characteristics of soot. Energy Fuels 2019;33:4515–30. https://doi.org/10.1021/acs.energyfuels.8b03841.
[20] Burwell JT. Survey of possible wear mechanisms. Wear 1957;1:119–41. https://doi.org/10.1016/0043-1648(57)90005-4.
[21] Dwyer-Joyce RS. The Life Cycle of a Debris Particle. Tribology and Interface Engineering Series. Elsevier Masson SAS; 2005. p. 681–90. https://doi.org/10.1016/S0167-8922(05)80070-7.
[22] Abdulqadir LB. Investigation of the Effects of Soot on the Wear of Automotive Engine Components. University of Sheffield; 2017.
[23] Berbezier I, Martin JM, Kapsa P. The role of carbon in lubricated mild wear. Tribol Int 1986;19:115–22. https://doi.org/10.1016/0301-679X(86)90016-2.
[24] Corso S, Adamo R. The Effect of Diesel Soot on Reactivity of Oil Additives and Valve Train Materials. SAE Int; 1984. https://doi.org/10.4271/841369.
[25] Antusch S, Dienwiebel M, Nold E, Albers P, Spicher U, Scherge M. On the tribochemical action of engine soot. Wear 2010;269:1–12. https://doi.org/10.1016/j.wear.2010.02.028.
[26] F.G. Rounds, Carbon: Cause of Diesel Engine Wear?, in: SAE Transactions, 1977: pp. 2870–2881. https://doi.org/10.4271/770829.
[27] F.G. Rounds, Soots from Used Diesel Engine Oils - Their Effects on Wear as Measured in 4-Ball Wear Tests, in: SAE Technical Papers, 1981. https://doi.org/10.4271/810499.
[28] Bagi S, Sharma V, Patel M, Aswath PB. Effects of diesel soot composition and accumulated vehicle mileage on soot oxidation characteristics. Energy Fuels 2016;30:8479–90. https://doi.org/10.1021/acs.energyfuels.6b01304.
[29] Motamen Salehi F, Morina A, Neville A. The effect of soot and diesel contamination on wear and friction of engine oil pump. Tribol Int 2017;115:285–96. https://doi.org/10.1016/j.triboint.2017.05.041.

[30] Motamen Salehi F, Morina A, Neville A. Zinc dialkyldithiophosphate additive adsorption on carbon black particles. Tribol Lett 2018;66:118. https://doi.org/10.1007/s11249-018-1070-6.
[31] Yahagi Y. Corrosive wear of diesel engine cylinder bore. Tribol Int 1987;20:365–73. https://doi.org/10.1016/0301-679X(87)90065-X.
[32] K. Akiyama, K. Masunaga, K. Kado, T. Yoshioka, Cylinder Wear Mechanism in an EGR-Equipped Diesel Engine and Wear Protection by the Engine Oil, SAE Technical Papers (1987). https://doi.org/10.4271/872158.
[33] Bae M, Tsuchiya K. A study on effects of recirculated exhaust gas upon wear of cylinder liner and piston in diesel engines. KSME Int J 2001;15:1524–32. https://doi.org/10.1007/BF03185742.
[34] Tortora AM, Zijlstra G, Veeregowda DH. Novel insight into tribology of carbon black soot particles in engine oil. Mater Perform Charact 2020;9:20200001. https://doi.org/10.1520/MPC20200001.
[35] Kontou A, Southby M, Morgan N, Spikes HA. Influence of dispersant and ZDDP on soot wear. Tribol Lett 2018;66:157. https://doi.org/10.1007/s11249-018-1115-x.
[36] Motamen Salehi F, Khaemba DN, Morina A, Neville A. Corrosive–abrasive wear induced by soot in boundary lubrication regime. Tribol Lett 2016;63:19. https://doi.org/10.1007/s11249-016-0704-9.
[37] Swapna MS, Saritha Devi H v, Raj V, Sankararaman S. Fractal and spectroscopic analysis of soot from internal combustion engines. Eur Phys J 2018;133:106. https://doi.org/10.1140/epjp/i2018-11918-y.
[38] Green DA, Lewis R. The effects of soot-contaminated engine oil on wear and friction: a review. Proc Inst Mech Eng, Part D: J Automob Eng 2008;222:1669–89. https://doi.org/10.1243/09544070JAUTO468.
[39] Uy D, Ford MA, Jayne DT, O'Neill AE, Haack LP, Hangas J, et al. Characterization of gasoline soot and comparison to diesel soot: Morphology, chemistry, and wear. Tribol Int 2014;80:198–209. https://doi.org/10.1016/j.triboint.2014.06.009.
[40] la Rocca A, di Liberto G, Shayler PJ, Fay MW. The nanostructure of soot-in-oil particles and agglomerates from an automotive diesel engine. Tribol Int 2013;61:80–7. https://doi.org/10.1016/j.triboint.2012.12.002.
[41] Clague ADH, Donnet JB, Wang TK, Peng JCM. A comparison of diesel engine soot with carbon black. Carbon N Y 1999;37:1553–65. https://doi.org/10.1016/S0008-6223(99)00035-4.
[42] Lapuerta M, Martos FJ, Herreros JM. Effect of engine operating conditions on the size of primary particles composing diesel soot agglomerates. J Aerosol Sci 2007;38:455–66. https://doi.org/10.1016/j.jaerosci.2007.02.001.
[43] Virtanen AKK, Ristimäki JM, Vaaraslahti KM, Keskinen J. Effect of Engine Load on Diesel Soot Particles. Environ Sci Technol 2004;38:2551–6. https://doi.org/10.1021/es035139z.
[44] Esangbedo C, Boehman AL, Perez JM. Characteristics of diesel engine soot that lead to excessive oil thickening. Tribol Int 2012;47:194–203. https://doi.org/10.1016/j.triboint.2011.11.003.
[45] E.A. Bardasz, V.A. Carrick, H.F. George, M.M. Graf, R.E. Kornbrekke, S.B. Pocinki, Understanding soot mediated oil thickening through designed experimentation part 4: Mack T-8 test, SAE Technical Papers (1997). https://doi.org/10.4271/971693.
[46] Covitch MJ, Humphrey BK, Ripple DE. Oil thickening in the mack T-7 engine test-fuel effects and the influence of lubricant additives on soot aggregation. SAE Trans 1985;94:839–54. ⟨https://www.jstor.org/stable/44467465⟩.
[47] D5185–18 Standard Test Method for Multielement Determination of Used and Unused Lubricating Oils and Base Oils by Inductively Coupled Plasma Atomic Emission Spectroscopy (ICP-AES), ASTM International, 2018.
[48] ASTM International, Standard Test Method for Acid Number of Petroleum Products by Potentiometric Titration D664, (2018). https://doi.org/10.1520/D0664–18E02.
[49] ASTM International, Standard Test Method for Base Number of Petroleum Products by Potentiometric Perchloric Acid Titration D2896, (2021). https://doi.org/10.1520/D2896–21.
[50] ASTM International, Standard Test Method for Base Number Determination by Potentiometric Hydrochloric Acid Titration D4739, (2017). https://doi.org/10.1520/D4739–17.
[51] ASTM International, Standard Test Method for Evaluation of Diesel Engine Oils in T-8 Diesel Engine D5967, (2021). https://doi.org/10.1520/D5967–21.
[52] ASTM International, Standard Practice for Condition Monitoring of In-Service Lubricants by Trend Analysis Using Fourier Transform Infrared (FT-IR) Spectrometry E2412, (2010). https://doi.org/10.1520/E2412–10R18.
[53] ASTM International, Testing of lubricants - Determination of oxidation and nitration of used motor oils - Infrared spectrometric method DIN51453, (2004).
[54] ASTM International, Standard Test Method for Kinematic Viscosity of Transparent and Opaque Liquids (and Calculation of Dynamic Viscosity) D445, (2021). https://doi.org/10.1520/D0445–21E02.
[55] ASTM International, Standard Test Method for Apparent Viscosity of Engine Oils and Base Stocks Between-10 °C and-35 °C Using Cold-Cranking Simulator D5293, (2020). https://doi.org/10.1520/D5293–20.
[56] ASTM International. D4683-20 Standard Test Method for Measuring Viscosity of New and Used Engine Oils at High Shear Rate and High Temperature by Tapered Bearing Simulator Viscometer At 150 ° C. West Conshohocken, PA: ASTM International; 2020. https://doi.org/10.1520/D4683-20.
[57] Pagkalis K, Spikes H, Jelita Rydel J, Ingram M, Kadiric A. The influence of steel composition on the formation and effectiveness of anti-wear films in tribological contacts. Tribol Lett 2021;69:75. https://doi.org/10.1007/s11249-021-01438-6.
[58] HFRR - PCS Instruments, (n.d.). ⟨https://pcs-instruments.com/product/hfrr/⟩ (accessed September 13, 2022).
[59] Olfert J, Rogak S. Universal relations between soot effective density and primary particle size for common combustion sources. Aerosol Sci Technol 2019;53:485–92. https://doi.org/10.1080/02786826.2019.1577949.
[60] M.T. Devlin, W.Y. Lam, T.F. McDonnell, Critical Oil Physical Properties that Control the Fuel Economy Performance of General Motors Vehicles, in: 1998. https://doi.org/10.4271/982503.
[61] C. Bovington, V. Anghel, H.A. Spikes, 1Predicting Sequence VI and VIA Fuel Economy from Laboratory Bench Tests, in: 1996. https://doi.org/10.4271/961142.
[62] Benchaita MT, Lockwood FE. Reliable model of lubricant-related friction in internal combustion engines. Lubr Sci 1993;5:259–81. https://doi.org/10.1002/ls.3010050402.
[63] Yang S, Reddyhoff T, Spikes H. Influence of lubricant properties on ARKL temperature rise and transmission efficiency. Tribology Trans 2013;56:1119–36. https://doi.org/10.1080/10402004.2013.804968.
[64] Grahn M, Johansson K, Vartia C, McKelvey T. 1A Structure and Calibration Method for Data-Driven Modeling of NO X and Soot Emissions from a Diesel Engine. In: Technical Papers SAE, editor. SAE International; 2012. https://doi.org/10.4271/2012-01-0355.
[65] Anscombe FJ. Graphs in statistical analysis. Am Stat 1973;27:17–21. https://doi.org/10.2307/2682899.
[66] Kagaya M. Study on diesel soot (Part 2) discussion concerning the mechanism of valve train wear by diesel soot. J Jpn Pet Inst 1997;40:488–93. https://doi.org/10.1627/jpi1958.40.488.
[67] Sato T, Saito H, Korematsu K, Tanaka J. Study on Wear of Piston Rings in Diesel Engines With Exhaust Gas Recirculation. Volume 3: Engine Systems: Lubrication, Wear, Components, System Dynamics, and Design. American Society of Mechanical Engineers; 2001. p. 39–45. https://doi.org/10.1115/ICES2001-132.
[68] Spikes H. The history and mechanisms of ZDDP. Tribol Lett 2004;17:469–89. https://doi.org/10.1023/B:TRIL.0000044495.26882.b5.
[69] Yagishita K, Igarashi J. ^{31}P NMR and mass spectrometric studies of the reaction of zinc dialkyldithiophosphates with cumene hydroperoxide. (Part 1). Kinetics and mechanisms of the initial homolytic reaction. J Jpn Pet Inst 1995;38:374–83. https://doi.org/10.1627/jpi1958.38.374.
[70] Masuko M, Ohkido T, Suzuki A, Ueno T. Fundamental study of changes in friction and wear characteristics due to ZnDTP deterioration in simulating engine oil degradation during use. : Tribology Ser 2003:359–66. https://doi.org/10.1016/S0167-8922(03)80063-9.
[71] Wan Y, Suominen Fuller ML, Kasrai M, Bancroft GM, Fyfe K, Torkelson JR, et al. Effects of detergent on the chemistry of tribofilms from ZDDP: studied by X-ray absorption spectroscopy and XPS. In: Dowson D, Priest M, Dalmaz G, Lubrecht AA, editors. Tribology Series. Elsevier Science & Technology; 2002. p. 155–66. https://doi.org/10.1016/S0167-8922(02)80017-7.
[72] Yu LG, Yamaguchi ES, Kasrai M, Bancroft GM. The chemical characterization of tribofilms using XANES — Interaction of nanosize calcium-containing detergents with zinc dialkyldithiophosphate. Can J Chem 2007;85:675–84. https://doi.org/10.1139/v07-045.
[73] Mourhatch R, Aswath PB. Tribological behavior and nature of tribofilms generated from fluorinated ZDDP in comparison to ZDDP under extreme pressure conditions—Part 1: structure and chemistry of tribofilms. Tribol Int 2011;44:187–200. https://doi.org/10.1016/j.triboint.2010.10.018.
[74] Ueda M, Kadiric A, Spikes H. Influence of steel surface composition on ZDDP tribofilm growth using ion implantation. Tribol Lett 2021;69:62. https://doi.org/10.1007/s11249-021-01436-8.